Low-energy fusion caused by an interference

B. Ivlev
Universidad Autónoma de San Luis Potosí, San Luis Potosi, Mexico
(Received 5 July 2012; revised manuscript received 17 February 2013; published 20 March 2013)

Fusion of two deuterons at room-temperature energy is studied. The nuclei are in vacuum with no connection to any external source (electric or magnetic field, illumination, surrounding matter, traps, etc.) which may accelerate them. The energy of the two nuclei is conserved and remains small during the motion through the Coulomb barrier. The penetration through this barrier, which is the main obstacle for low-energy fusion, strongly depends on a form of the incident flux on the Coulomb center at large distances from it. In contrast to the usual scattering, the incident wave is not a single plane wave but the certain superposition of plane waves of the same energy and various directions; for example, a convergent conical wave. As a result of interference, the wave function close to the Coulomb center is determined by a cusp caustic which is probed by de Broglie waves. The particle flux gets away from the cusp and moves to the Coulomb center providing a not negligible probability of fusion (cusp driven tunneling). Getting away from a caustic cusp also occurs in optics and acoustics.

DOI: 10.1103/PhysRevC.87.034619 PACS number(s): 25.45.−z, 03.65.Xp, 03.65.Sq

I. INTRODUCTION

The aspects of nuclear fusion are discussed, for instance, in Refs. [1–10] and references therein. Here we outline principal phenomena associated with nuclear fusion. The main difficulty is getting the nuclei close enough to fuse since they should overcome a high Coulomb barrier.

There are two ways to pass the Coulomb barrier: to accelerate the nuclei up to a high energy comparable with the barrier height (of the order of 1 MeV) or to pass the barrier via quantum tunneling. When the energy is not high, the probability of tunneling of the nuclei through the Coulomb barrier is extremely small according to the theory of Wentzel, Kramers, and Brillouin (WKB) [11]. So only high-energy nuclei can fuse.

Therefore, use of high-energy nuclei is the leading idea of fusion technique. We mention an acceleration of initially cold deuterons by a strong electric field using a pyroelectric crystal [5].

It is surprising to claim that *two bare deuterons*, that are isolated from everything, *of room-temperature energy* are able, in principle, to penetrate the Coulomb barrier with a not small probability and to subsequently fuse. This statement is counterintuitive. A tennis ball cannot penetrate through a brick wall. This correlates with the usual underbarrier physics led by the philosophy of addition of probabilities but not amplitudes. The proposed phenomenon of barrier penetration is based ultimately on interference that is on addition of amplitudes. The related nuclear reaction can be called *coherent fusion*.

We really deal with two low-energy nuclei in vacuum. There are no external sources (electric or magnetic field, illumination, surrounding matter, traps, etc.) which may accelerate them. The energy of the two nuclei, in the system of center of mass, is conserved and remains small during the motion through the Coulomb barrier. This is a substantial difference from usual schemes to push in action a mechanism of low-energy fusion by some local heating or acceleration of nuclei.

The conventional scattering problem is a study of reflection of the incident flux which is a plane wave coming from large distances [11]. Coulomb field scattering relates to the Rutherford formula and the wave function is exponentially small at the center.

What happens when the incident flux at large distances is not just a single plane wave?

The wave function close to the Coulomb center can be substantially modified when the incident flux is a superposition of plane waves with the same energy in various directions; for example, a convergent conical wave. In this case classical trajectories are reflected, due to Coulomb forces, from a certain surface surrounding the cone axis. This surface is called caustic [12] and it is terminated by the cusp directed to the center. Classical trajectories fill out the space restricted by the caustic surface. Each incident trajectory reflects from the caustic surface, continues inside, and pierces its opposite part. So the space outside the caustic is not an absolute shadow from the classical standpoint.

Classical trajectories, which pierce the surface of the cusp caustic, do not reach the Coulomb center since they are reflected from another caustic closer to the center. So the Coulomb center is in the absolute shadow from the classical standpoint. Otherwise it would be strange to have the center be reachable within classical physics.

Unlike classical physics, a caustic shadow is not completely "empty" due to an exponential decay of the wave function outside the caustic surface [12]. The proper outer flux of the cusp caustic is directed along it. When the flux reaches the cusp it gets away from it and moves towards the center. It pierces the caustic which reflects the above classical flux propagated after piercing the cusp caustic. Then it reaches the Coulomb center providing a not exponentially small probability of tunneling. The cusp driven flux does not exist in classical physics. The analogous flux, getting away from a caustic cusp, is also formed in optics and acoustics. See also Refs. [13,14].

In this paper the exact solution of the Coulomb problem is used. In the Coulomb field the variables are separated in parabolic coordinates [11] and the solution is a product of two wave functions. They depend on an arbitrary parameter β indicating a redistribution of the total constant energy between two subsystems. Therefore the wave function is an infinite

superposition of such products with different β corresponding to an integration along some path in the plane of complex β.

The result is determined by analytical properties in the β plane where the certain points relate to saddle point integrations. Each saddle point corresponds to a solution of the Hamilton-Jacobi equation [11,15]. But not every solution of this equation is physical. The exact analytical solution allows us to establish whether a particular saddle contributes to the total integration. Some saddles are irrelevant since they are masked by other branches of larger amplitude.

The phenomenon of interference in tunneling was already proposed in Refs. [16–18]. Multidimensional tunneling was studied, in particular, in Refs. [19–27]. Influence of interference on tunneling through nonstationary barriers was studied in Refs. [28,29]. The role of interference in α decay was studied in Ref. [30].

Experimental conditions to form the required incident flux are briefly discussed in Sec. XI.

Let us summarize what is proposed in this paper. We assume (i) there is a conical convergent flux of particles (not a plane wave) on the static repulsive Coulomb center, (ii) the Coulomb field is the only interaction, (iii) the particle energy is fixed and low resulting in an exponentially small WKB probability to reach the Coulomb center. We conclude that (i) the cusp caustic is formed, (ii) the flux gets away from the cusp and moves along the narrow channel toward the Coulomb center, and (iii) the probability to reach the center is not exponentially small.

II. GENERAL VIEW

Two examples of nuclear fusion are below. The deuterium-deuterium fusion occurs by the scheme

$$ {}^2_1\mathrm{H} + {}^2_1\mathrm{H} \to {}^3_2\mathrm{He} + n + 3.27\ \mathrm{Mev}. \tag{1}$$

The deuterium-tritium fusion releases more energy,

$$ {}^2_1\mathrm{H} + {}^3_1\mathrm{H} \to {}^4_2\mathrm{He} + n + 17.59\ \mathrm{Mev}. \tag{2}$$

The problem of nuclear fusion can be separated by two steps. The first step is overcoming the Coulomb barrier by two nuclei with masses M_1 and M_2. When the inter-nuclear distance is larger than $R_0 \sim 10^{-13}$ cm one can ignore nuclear forces, considering only tunneling through the Coulomb barrier. This process determines the local nuclear densty on the outer border of the region $R < R_0$. The second step is a subsequent nuclear fusion on the short distance R_0. When the above nuclear density is not small the probability of the fusion is also not small. Our goal is not to calculate the exact fusion probability but to show that it is not exponentially small. For this purpose, the consideration of the Coulomb tunneling is sufficient.

The Coulomb process is a motion of a particle with the reduced mass $M = M_1M_2/(M_1 + M_2)$ described by the Schrödinger equation

$$ -\frac{\hbar^2}{2M}\frac{\partial^2\psi}{\partial\vec{R}^2} + \frac{e^2}{R}\psi = E\psi, \tag{3}$$

where R is the internuclear distance [11]. Below we measure length in the units of $2e^2/E$. The wave function can be written in the form

$$ \psi = \exp(iB\sigma), \tag{4}$$

where σ satisfies the equation

$$ \frac{1}{4}\left(\frac{\partial\sigma}{\partial\vec{R}}\right)^2 + \frac{1}{2R} - \frac{i}{4B}\frac{\partial^2\sigma}{\partial\vec{R}^2} = 1. \tag{5}$$

The parameter

$$ B = \frac{e^2}{\hbar c}\sqrt{\frac{2Mc^2}{E}} \tag{6}$$

is supposed to be large, which corresponds to semiclassical approximation. In this case one can ignore the last term in Eq. (5) and it becomes the Hamilton-Jacobi equation when σ is the classical action divided by $\hbar B$ [11,15].

In a spherically symmetric case the first term in Eq. (5) is just $(\partial\sigma/\partial R)^2/4$. The wave function exponentially decays inside the Coulomb barrier. Accordingly, the imaginary part of σ, related to a motion under the barrier, is

$$ \sigma = i\sqrt{2}\int_{R_0}^{1/2} dR\sqrt{\frac{1}{R} - 2} \simeq \frac{i\pi}{2}, \tag{7}$$

where we ignore the distance R_0 which is short compared to scales of the Coulomb motion. Equation (7) follows from the WKB approximation The probability of fusion is the probability of overcoming the Coulomb barrier,

$$ w = \left|\frac{\psi(R_0)}{\psi(\infty)}\right|^2 \sim \exp(-\pi B). \tag{8}$$

One can estimate the fusion probability (8), for example, for the reaction (1). In this case the reduced mass is $M = M_D/2$ where the deuteron mass is defined as $M_Dc^2 \simeq 1.87 \times 10^9$ eV. The nuclear Bohr radius is $\hbar^2/Me^2 \simeq 2.88 \times 10^{-12}$ cm. At the energy of two deuterons $E = T$, where $T = 300\ \mathrm{K} \simeq 2.58 \times 10^{-2}$ eV relates to room temperature, and the de Broglie wavelength is $\lambda = 2\pi\hbar/\sqrt{2M_DE} \simeq 1.26$ Å. Two deuterons enter the Coulomb barrier at the distance $e^2/E \simeq 557$ Å between them. With these parameters one can estimate $\pi B \simeq 6174.9$. This corresponds to the probability $w \sim 10^{-2682}$ which is in accordance with usual estimates for low-energy fusion.

III. SCATTERING BY THE COULOMB CENTER

The above estimate of nonphysically small probability of low-energy fusion corresponds to the usual WKB approximation. For a spherically symmetric incident flux the problem is a generic one-dimensional case since radial and spherical parts of the wave function are separated.

There is another remarkable case of variables separation in the Coulomb field. It occurs in parabolic coordinates

$$ \xi = \sqrt{r^2 + z^2} + z, \quad \eta = \sqrt{r^2 + z^2} - z. \tag{9}$$

In this case the total wave function has the form

$$ \psi(\xi, \eta) = f(\xi)\varphi(\eta)\exp(im\Phi), \tag{10}$$

where Φ is the azimuthal angle and m is the magnetic quantum number. The use of spherical coordinates is less convenient for our purposes due to the discrete summation on azimuthal quantum number l as in the problem of Regge poles [31]. Below we consider an axially symmetric case when $m = 0$ and the Schrödinger equation has the form

$$-\frac{1}{4B^2 r}\frac{\partial}{\partial r}\left(r\frac{\partial\psi}{\partial r}\right)-\frac{1}{4B^2}\frac{\partial^2\psi}{\partial z^2}+\frac{\psi}{2\sqrt{r^2+z^2}}=\psi. \quad (11)$$

In the parabolic coordinates the Schrödinger equation reads

$$-\frac{1}{B^2(\xi+\eta)}\left[\frac{\partial}{\partial\xi}\left(\xi\frac{\partial\psi}{\partial\xi}\right)+\frac{\partial}{\partial\eta}\left(\eta\frac{\partial\psi}{\partial\eta}\right)\right]+\frac{\psi}{\xi+\eta}=\psi. \quad (12)$$

If we express the wave function as $\psi = \exp(iB\sigma)$, one can obtain from Eq. (12)

$$\xi\left(\frac{\partial\sigma}{\partial\xi}\right)^2-\frac{i}{B}\frac{\partial}{\partial\xi}\left(\xi\frac{\partial\sigma}{\partial\xi}\right)+\eta\left(\frac{\partial\sigma}{\partial\eta}\right)^2 -\frac{i}{B}\frac{\partial}{\partial\eta}\left(\eta\frac{\partial\sigma}{\partial\eta}\right)+1=\xi+\eta. \quad (13)$$

After separation of variables the parts f and φ in Eq. (10) obey the equations [11]

$$-\frac{1}{B^2\xi}\frac{\partial}{\partial\xi}\left(\xi\frac{\partial f}{\partial\xi}\right)+\frac{1+\beta}{\xi}f=f, \quad (14)$$

$$-\frac{1}{B^2\eta}\frac{\partial}{\partial\eta}\left(\eta\frac{\partial\varphi}{\partial\eta}\right)-\frac{\beta}{\eta}\varphi=\varphi, \quad (15)$$

where β is a constant connected with the variable separation.

Each of Eqs. (14) and (15) has two independent solutions. The WKB limits of these solutions are [11]

$$\varphi_{\mp}(\eta,\beta)=\frac{[\eta(\eta+\beta)]^{-1/4}}{2\sqrt{\mp iB\pi}}\exp\left(\mp iB\int_0^{\eta}d\eta_1\sqrt{1+\frac{\beta}{\eta_1}}\right) \quad (16)$$

and analogously

$$f_{\mp}(\xi,\beta)=\frac{[\xi(\xi-1-\beta)]^{-1/4}}{2\sqrt{\mp iB\pi}} \times\exp\left(\mp iB\int_{1+\beta}^{\xi}d\xi_1\sqrt{1-\frac{1+\beta}{\xi_1}}\right). \quad (17)$$

Equations (16) and (17) are valid when the phases are not small.

The velocity field can be studied by Newtonian trajectories. According to classical mechanics [15], velocities in the ξ and η directions are proportional to $\sqrt{1-(1+\beta)/\xi}$ and $\sqrt{1+\beta/\eta}$ respectively. This sets a velocity field in the plane $\{\xi,\eta\}$. Each point in the plane $\{\xi,\eta\}$ belongs to one or a few classical trajectories $\eta(\xi)$.

In the usual scattering problem the incident flux is solely a plane wave from large positive z. This situation corresponds to $\beta = -i/B$ ($\beta \simeq 0$ in the semiclassical approximation) when the exact solution of Eq. (15) is $\varphi_+ = \exp(iB\eta)$ [11]. The combination $f_-(\xi)\varphi_+(\eta)$ results in the incident plane wave $\psi \sim \exp(-2iBz)$ at large positive z. Analogously, the combination $f_+(\xi)\varphi_+(\eta)$ leads to the scattered wave $\psi \sim \exp(2iB\sqrt{r^2+z^2})$ far from the center.

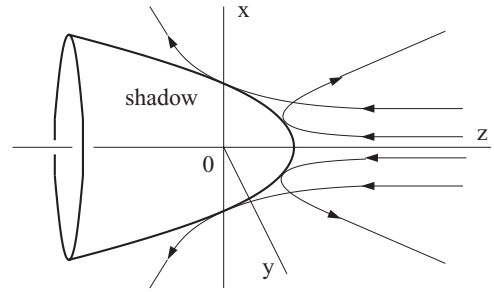

FIG. 1. The flux on the Coulomb center (zero coordinates) is reflected from the caustic surface defined by Eq. (18). Four trajectories from the infinite set are shown.

Classical trajectories are shown in Fig. 1. They are reflected from the caustic surface where the velocity $\partial\xi/\partial t = 0$ [12]. This happens at $\xi = 1+\beta \simeq 1$. See also Refs. [32,33] where properties of the caustic in Fig. 1 and associated wave functions are discussed. The caustic surface in Fig. 1 is axially symmetric, since $m = 0$, and, as follows from Eq. (9), is given by

$$2z = 1 - r^2. \quad (18)$$

Along the caustic the normal momentum is zero. The tangent momentum is real and is determined by $\sqrt{1+\beta/\eta} \simeq 1$. The wave function exponentially decays inside the shadow region in Fig. 1.

IV. FORMULATION OF THE PROBLEM

A. Exact wave functions

Below we explore superpositions of functions with different β:

$$\psi_I(\xi,\eta)=\int d\beta\exp(-iB\alpha\beta)f(\xi,\beta)\varphi(\eta,\beta), \quad (19)$$

$$\psi_{II}(\xi,\eta)=\int d\beta\exp(iB\alpha\beta)f(\eta,-1-\beta)\varphi(\xi,-1-\beta), \quad (20)$$

where α is a fixed positive parameter. In these equations

$$f(\xi,\beta)=i\exp(-iB\xi-i\pi b)F(b,1,2iB\xi), \quad (21)$$

where $2b = 1 - iB(1+\beta)$, and

$$\varphi(\eta,\beta)=i\exp(-iB\eta)F(a,1,2iB\eta), \quad (22)$$

where $2a = 1 + iB\beta$. The confluent hypergeometric function [11] is given by the series

$$F(a,1,s)=1+\frac{a}{(1!)^2}s+\frac{a(a+1)}{(2!)^2}s^2 +\frac{a(a+1)(a+2)}{(3!)^2}s^3+\cdots. \quad (23)$$

The total wave function is

$$\psi(\xi,\eta)=\psi_I(\xi,\eta)+\psi_{II}(\xi,\eta). \quad (24)$$

As shown below, the function ψ_I is exponentially small at $z < 0$ and the function ψ_{II} is exponentially small at $0 < z$.

At large ξ and η the functions (21) and (22) have their WKB forms,

$$f(\xi,\beta) \simeq f_-(\xi,\beta) + f_+(\xi,\beta), \tag{25}$$

$$\varphi(\eta,\beta) \simeq \varphi_-(\eta,\beta) + \varphi_+(\eta,\beta). \tag{26}$$

The wave function (26) corresponds to incident and reflected waves in the classically allowed region. In the classically forbidden region, smaller η, this wave function exponentially decays with the decrease of η. There is also the part exponentially increasing with the decrease of η. Both are of the same order at small η. This reminds us of a usual one-dimensional problem of reflection from a barrier where, as known, the Stokes phenomena are involved [34]. The same is valid for the wave function (25).

The wave function (22) is not singular at small η. At some fixed negative β the function $\varphi(\eta,\beta)$ has two branches, exponentially increasing and decreasing from the point $\eta = 0$.

B. Semiclassical approximation

According to Eqs. (17) and (16), there are four ($i = 1, 2, 3, 4$) branches of the wave function ψ_I (analogously, of ψ_{II}),

$$\psi_i = \int a_i \exp(iB\sigma_i) d\beta, \tag{27}$$

where the preexponential factors a_i are not important for the semiclassical approach used. σ_i are defined by the following:

$$\sigma_{2,3} = \mp \int_{1+\beta}^{\xi} \sqrt{1 - \frac{1+\beta}{\xi_1}}\, d\xi_1 + \int_0^{\eta} \sqrt{1 + \frac{\beta}{\eta_1}}\, d\eta_1 - i\alpha\beta \tag{28}$$

and $\sigma_{1,4} + i\alpha\beta = -(\sigma_{3,2} + i\alpha\beta)$.

The large parameter B provides validity of the semiclassical approximation, and the β integration can be done by the saddle method. This means that for each ξ and η one can determine a certain $\beta(\xi,\eta)$ from the condition $\partial\sigma_i/\partial\beta = 0$. For σ_1 this condition reads

$$\sqrt{\frac{\xi}{1+\beta}} + \sqrt{\frac{\xi}{1+\beta} - 1} = \left(\sqrt{\frac{\eta}{\beta} + 1} + \sqrt{\frac{\eta}{\beta}}\right) \exp(\alpha). \tag{29}$$

The analogous condition for σ_2 differs from Eq. (29) by the sign at $\sqrt{\eta/\beta}$. The condition for σ_3 differs from Eq. (29) by the sign of α. The condition for σ_4 is obtained to make both changes in Eq. (29).

The above semiclassical solutions also follow from the Hamilton-Jacobi equation. Equation (13) becomes this equation if we drop the second derivatives. The Hamilton-Jacobi equation in parabolic coordinates,

$$\frac{\xi}{\xi+\eta}\left(\frac{\partial\sigma}{\partial\xi}\right)^2 + \frac{\eta}{\xi+\eta}\left(\frac{\partial\sigma}{\partial\eta}\right)^2 + \frac{1}{\xi+\eta} = 1 \tag{30}$$

allows separation of the variables used above. Equations (28) for σ_i with the conditions (29) are equivalent to a general integral of the Hamilton-Jacobi equation (30) [15].

To obtain derivatives $\partial\sigma_i/\partial\xi$ and $\partial\sigma_i/\partial\eta$ one should differentiate in Eq. (28) with respect to the upper integration limits only. For σ_1, for example, we have

$$\frac{\partial\sigma_1(\xi,\eta)}{\partial\xi} = -\sqrt{1 - \frac{1+\beta(\xi,\eta)}{\xi}}, \tag{31}$$

$$\frac{\partial\sigma_1(\xi,\eta)}{\partial\eta} = -\sqrt{1 + \frac{\beta(\xi,\eta)}{\eta}}. \tag{32}$$

The Cartesian derivatives

$$\frac{\partial\sigma_i}{\partial z} = \frac{2}{\xi+\eta}\left(\xi\frac{\partial\sigma_i}{\partial\xi} - \eta\frac{\partial\sigma_i}{\partial\eta}\right) \tag{33}$$

and

$$\frac{\partial\sigma_i}{\partial r} = \frac{2\sqrt{\xi\eta}}{\xi+\eta}\left(\frac{\partial\sigma_i}{\partial\xi} + \frac{\partial\sigma_i}{\partial\eta}\right) \tag{34}$$

are proportional to classical velocities.

Now one can outline the problem. From Eq. (29) and its analogs one has to determine $\beta(\xi,\eta)$ and to insert it into Eq. (28) and its analogs. A semiclassical solution will be found.

V. CAUSTICS

A condition of applicability of the semiclassical approximation is well known. A wavelength should be a smooth function of coordinates [11]. In other words, quantum corrections to the Hamilton-Jacobi equation (30), which contain $(1/B)\partial^2\sigma/\partial\xi^2$ and $(1/B)\partial^2\sigma/\partial\eta^2$, should be small. There are various situations when those derivative are not small. First, it happens near a classical turning point where classical momenta ($\sim\partial\sigma/\partial\xi$) are proportional to the square root of the distance to this point.

In addition to that, the classical momentum can be nonzero but nevertheless its spatial derivative becomes infinite. As follows from Eqs. (31) and (32), this may happen when $\partial\beta/\partial\xi$ or $\partial\beta/\partial\eta$ become large. This condition specifies a certain surface, called caustic, in the three-dimensional space where classical trajectories are tangent to it [12]. In our case caustic surfaces have axial symmetry with respect to the z axis and one can study just caustic curves in the $\{r, z\}$ plane. The caustic condition can be obtained from Eq. (29) by the formal condition $\partial\xi/\partial\beta = 0$ at a fixed η. After a little algebra the caustic condition reads

$$\begin{aligned}\frac{2\xi}{1+\beta} &= 2(1+\beta)\cosh^2\alpha - \sinh^2\alpha \\ &\quad \pm \sinh\alpha\sqrt{\sinh^2\alpha + 4\beta(1+\beta)\cosh^2\alpha}, \\ \frac{2\eta}{\beta} &= 2\beta\cosh^2\alpha + \sinh^2\alpha \\ &\quad \mp \sinh\alpha\sqrt{\sinh^2\alpha + 4\beta(1+\beta)\cosh^2\alpha},\end{aligned} \tag{35}$$

which determines the caustic form $\eta(\xi)$ to exclude β in these equations.

The upper sign in Eq. (35) relates to the branch σ_1 and produces the caustics D_1 and B_1 in Fig. 2. The lower sign in Eq. (35) relates to the branch σ_3 and results in the caustics D_3 and B_3 in Fig. 2.

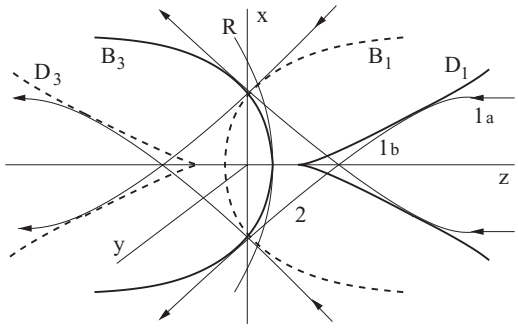

FIG. 2. Distribution of the particle flux associated with the wave function ψ_I. Caustic surfaces are axially symmetric with respect to the z axis. The curves represent intersection of caustics and the $\{x, z\}$ plane. The caustic D_1 touches the z axis at the point z_s. The caustic B_3 intersects the z axis at the point $z = 1/2$. On the dashed caustics ψ_I is exponentially small. On the curve R the branch ψ_2 is converted into ψ_3.

The caustic D_1 at small r corresponds to small β and to large β at large r. One can easily obtain the shape of the caustic D_1 in limiting cases,

$$r = \frac{4\sqrt{2}}{\sinh 2\alpha}\left(\frac{z - z_s}{3}\right)^{3/2}, \quad (z - z_s) \ll z_s, \tag{36}$$

$$r = \frac{z}{\sinh\alpha}\left(1 - \sqrt{\frac{2z_s}{z\tanh\alpha}}\right), \quad z_s \ll z, \tag{37}$$

where $2z_s = \cosh^2\alpha$. The caustic B_1 corresponds to $\beta < -1$. At small r it should be $(-1 - \beta) \ll 1$ and at large r the parameter $(-\beta)$ is large. The form of the caustic B_1 in limiting cases is

$$r = \sinh\alpha\sqrt{1 + 2z}, \quad (2z + 1) \ll 1, \tag{38}$$

$$r = \frac{z}{\sinh\alpha}\left(1 + \sqrt{\frac{2z_s}{z\tanh\alpha}}\right), \quad 1 \ll z. \tag{39}$$

The pair of caustics $\{D_3, B_3\}$ is a mirror reflection of the pair $\{D_1, B_1\}$ with respect to the x axis as shown in Fig. 2. The caustics D_1 and D_3 have a cusp shape close to the points $z = \pm z_s$.

Along caustics $\mathrm{Im}\,\sigma = \mathrm{const}$ and the momentum is tangent to the caustic; that is, along each caustic

$$\left(\frac{\partial \mathrm{Re}\sigma}{\partial r}\right) = \left(\frac{\partial \mathrm{Re}\sigma}{\partial z}\right)\frac{\partial r}{\partial z}. \tag{40}$$

The incident flux at large distances from the Coulomb center determines a form of the cusp caustic which can be of the type $x^2 + y^2 \sim (z - z_s)^{k+1}$ [35]. In our case $k = 2$. It is interesting to use other types of incident flux to obtain higher k, which promises to yield an enhanced effect. Also it is likely that each of the caustic pairs, $\{D_1, B_1\}$ and $\{D_3, B_3\}$, originates from a common source. This research is outside the framework of this paper and will be done in the near future.

VI. CLASSICAL FLUX ASSOCIATED WITH ψ_I

In this section we specify the velocity field associated with the wave function ψ_I. First, we focus on the region $(z - z_s)$, $r \ll 1$ where the caustic D_1 in Fig. 2 is about to touch the z axis. In this case the parameter β is small and Eq. (29) can be written in the form

$$\beta_1^{3/2} + \frac{z_s - z}{z_s}\sqrt{\beta_1} + r\sqrt{\frac{2}{z_s}}\tanh\alpha = 0, \tag{41}$$

which is cubic with respect to $\sqrt{\beta_1}$. We ascribe the index "1" to β to emphasize its connection to the branch σ_1.

Two physical solutions of Eq. (41) at $(z - z_s) \ll 1$ are

$$\beta_{1a,b} = \frac{z - z_s}{3z_s}\left[1 \mp \sqrt{\frac{1}{3} - \left(\frac{3r\sinh 2\alpha}{4\sqrt{2}}\right)^2\left(\frac{1}{z - z_s}\right)^3}\right] \tag{42}$$

which are valid close to the caustic D_1; that is, when the square root in Eq. (42) is small. Two signs of the square root provide two opposite velocities normal to the caustic D_1 from the classical side. Close to the z axis

$$\beta_{1a} = \left(\frac{r\sinh\alpha}{z - z_s}\right)^2, \quad \beta_{1b} = \frac{z - z_s}{z_s}, \quad r^2 \ll (z - z_s)^3 \ll 1 \tag{43}$$

Now it easily follows from Eq. (29) that

$$\beta_{1a} = \frac{r^2}{8z}\left(\frac{\sqrt{2z}\sinh\alpha + \sqrt{2z - 1}\cosh\alpha}{z - z_s}\right)^2,$$
$$\beta_{1b} = \frac{z - z_s}{z_s} - \frac{rz\sqrt{2}\tanh\alpha}{z_s\sqrt{z - z_s}}, \quad r^2 \ll (z - z_s)^3. \tag{44}$$

As one can see, Eqs. (44) turn into Eqs. (43) when z is close to z_s.

A. Incident flux

Now one can analyze what happens to the incident flux (from the right in Fig. 2). It is described by the action σ_{1a} where the index a means that one has to substitute β_{1a} in Eq. (28) for σ_1. As follows from Eqs. (29), (33), and (34), at z not too close to z_s

$$\frac{\partial\sigma_{1a}}{\partial z} = -2\sqrt{1 - \frac{1}{2z}}, \quad r \ll 1, \quad z_s < z \tag{45}$$

$$\frac{\partial\sigma_{1a}}{\partial r} = -\frac{r}{z}\left[\sqrt{1 - \frac{1}{2z}} + \sqrt{1 + \left(\frac{\sqrt{2z}\sinh\alpha + \sqrt{1 - 2z}\cosh\alpha}{2(z - z_s)}\right)^2}\right]. \tag{46}$$

It is instructive to consider σ_1 on a classical trajectory which is just a curve in the entire space. The trajectory $1a$, associated with the branch σ_{1a}, is shown in Fig. 2. Trajectories of the type $1a$ do not intersect the z axis since, according to Eq. (46), the momentum normal to this axis becomes zero on it.

B. Flux associated with the caustic D_1

The trajectory $1a$ is reflected from the caustic D_1 and after reflection becomes the trajectory $1b$ as shown in Fig. 2. The related branch is σ_{1b}; that is, σ_1 with the above β_{1b}. As follows from Eqs. (29), (33), and (34), at $z_s < z$

$$\frac{\partial\sigma_{1b}}{\partial z} = -2\tanh\alpha - \frac{r}{z}\sqrt{\frac{z_s}{2z(z-z_s)}}, \quad r \ll 1,$$
$$\frac{\partial\sigma_{1b}}{\partial r} = -\sqrt{\frac{2(z-z_s)}{zz_s}} + \frac{rz_s\tanh\alpha}{z(z-z_s)}. \tag{47}$$

If we ignore a narrow region close to the z axis where the semiclassical approach is not valid, one can say that the trajectory $1b$ intersects the z axis since the momentum, normal to this axis, is finite.

After intersection of the z axis, the trajectory $1b$ turns into the trajectory 2 marked in Fig. 2. The related $\partial\sigma_2/\partial z$ and $\partial\sigma_2/\partial r$ differ from Eq. (47) by the sign of the square roots. This description of the branch 2 is valid for $r \ll 1$ and $z_s < z$. At $1/2 < z < z_s$ and $r \ll 1$, $\partial\sigma_2/\partial z$ has the same form (45) but $\partial\sigma_2/\partial r$ differs from Eq. (46) by the sign of the second square root. Since $\partial\sigma_2/\partial r$ is zero at $r = 0$, the part σ_2 behaves as a one-dimensional one on the z axis. Namely, it is related to the classical turning point $z = 1/2$ where the caustic B_3 intersects the z axis.

C. Branch conversion

Let us consider one of the functions ψ_I (19) which contains $f_-(\xi)[\varphi_-(\eta) + \varphi_+(\eta)]$. The sum of two φ functions has no logarithmic singularity at small η. In terms of the notation (27), this function is $\psi_1 + \psi_2$. As follows from Sec. VI, the branch ψ_2 can be calculated by the saddle point β integration (semiclassical approximation) to the right of a certain curve R in Fig. 2 where two branches, ψ_2 and ψ_3, merge due to the condition $\partial\sigma_{2,3}/\partial\xi = 0$.

The condition of the curve R, $\xi = 1 + \beta$, and equations of the type (29) but for $i = 2, 3$ yield $\beta = \eta/\sinh^2\alpha$. As a result, the curve R in Fig. 2 is determined by the form $\xi_R(\eta) = 1 + \eta/\sinh^2\alpha$ or

$$r_R(z) = \frac{\sinh\alpha}{\sinh^2\alpha - 1}\sqrt{(1-2z)(\sinh^2\alpha - 2z)}. \tag{48}$$

We consider $1 < \sinh\alpha$. Close to the curve R, tangent derivatives are $\partial\sigma_{2,3}/\partial\eta = 1/\tanh\alpha$. The derivative $\partial\sigma/\partial\xi \sim (\xi - \xi_R)$ corresponds to ψ_2 to the right of the curve R ($\xi_R < \xi$) and to ψ_3 to the left of the curve R ($\xi < \xi_R$).

In other words, Eq. (29) for ψ_2 does not have a solution to the left from the curve R (no saddle point). From the semiclassical standpoint, ψ_2 disappears to the left from the curve R turning into ψ_3. Note that the curve R is not a caustic.

VII. CHANNEL FORMATION

The flux, considered in Sec. VI, exists in the classical limit. But there is also a specific flux which disappears in classical mechanics. This flux is collected from the thin layer on the outer surface of the caustic D_1. In classical physics such a layer does not exist. Then the flux gets away from the cusp and moves toward the Coulomb center along a certain channel. In this section we study how the channel is formed.

A. Semiclassical description of the channel

At $z_s > z \sim 1$ equations can be formally obtained from Eq. (47),

$$\frac{\partial\sigma_1}{\partial z} = -2\tanh\alpha - \frac{ir}{z}\sqrt{\frac{z_s}{2z(z_s-z)}}, \quad r \ll 1$$
$$\frac{\partial\sigma_1}{\partial r} = i\sqrt{\frac{2(z_s-z)}{zz_s}} - \frac{rz_s\tanh\alpha}{z(z_s-z)}. \tag{49}$$

Outside the caustic D_1 one can drop the index b. At small r and z close to the cusp point z_s the action (49) can be written in the form

$$\sigma_1 = -2z\tanh\alpha + \frac{ir}{z_s}\sqrt{2(z_s-z)}. \tag{50}$$

We see that the branch ψ_1 decays inside the shadow of the caustic D_1 and also decays away from the z axis. So Eqs. (49) and (50) describe the particle flux propagated toward the Coulomb center along a narrow channel. The channel exists even in the classically forbidden region close to the Coulomb center. This conclusion is based on the semiclassical approximation and requires a more rigorous justification. Indeed, formally also another branch exists which differs from Eqs. (49) and (50) by the sign of the imaginary part in the action. This branch would destroy the construction of the channel. What happens to this branch?

B. Solution for the channel

The flux to the left from the cusp in Fig. 2 is described by the wave function (19) when in Eq. (25) only the part f_- is chosen:

$$\psi_I(\xi,\eta) = \int_C d\beta f_-(\xi,\beta)\exp\left[-iB(\alpha\beta+\eta)\right] \times F\left(\frac{1+iB\beta}{2}, 1, 2iB\eta\right). \tag{51}$$

Equation (51) corresponds to the form $\psi_1 + \psi_2$ according to the definition (27).

1. Integration contour

In the formula (19) the integration contour C should be properly chosen. This can be done on the basis of analytical properties of the integrand in Eq. (19) as a function of complex β.

Analytical properties can be obtained from the semiclassical form (25) and (17) which establishes the asymptote of the total wave function at large β, which is independent on ξ and η. This asymptote is the same for f_- and f_+ since they coincide in the classically forbidden region. The contour C can be chosen in a way to get at large β an exponentially

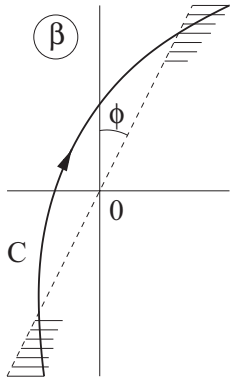

FIG. 3. The contour of integration C in the complex plane of β. The far ends of C are at the hatched regions where the wave function is exponentially small and vanishes.

small wave function. At large β the border, where the phase is real, corresponds to the condition $\mathrm{Re}\,\beta(-\pi/2 - i\alpha) = 0$. As a result, the far ends of the contour C should be at the hatched region in Fig. 3 that is to the right of the dashed line. The angle ϕ is given by

$$\phi = \arctan\frac{2\alpha}{\pi}. \tag{52}$$

2. Small $r < 1/B$

At small r and a finite z one can expand the function $\varphi(\eta, \beta)$ with respect to small $\eta \simeq r^2/2z$. After that one can obtain from Eq. (19)

$$\psi_I\left(2z, \frac{r^2}{2z}\right) = \int_C d\beta \left(1 - \frac{B^2\beta}{2z}r^2\right) f(\xi, \beta). \tag{53}$$

To perform the β integration in Eq. (53) one should know analytical properties of the confluent hypergeometric function (23) in the entire plane of complex a. We postpone this problem for the future.

3. Large $r > 1/B$

Saddle points in the complex plane of β are characteristics of the function $\exp(-iB\alpha\beta) f_-(\xi, \beta)\varphi_-(\eta, \beta)$ [Fig. 4(a)] and $\exp(-iB\alpha\beta) f_-(\xi, \beta)\varphi_+(\eta, \beta)$ [Fig. 4(b)]. The positions of these saddle points and directions of steepest descents, shown in Fig. 4, can be easily obtained from Sec. IV, and we omit details.

In Fig. 4(a) the saddle point is in the lower half-plane of β where $f_-(\xi, \beta)$, as a function of β, dominates $f_+(\xi, \beta)$ [11,34]. In Fig. 4(a) the integration path naturally matches the direction of steepest descent. This results in the saddle point contribution. The related part of the wave function decreases from the z axis according to the semiclassical approach developed above.

A different scenario takes place in Fig. 4(b) where the saddle point is in the upper half-plane of the complex β. In this half-plane $f_-(\xi, \beta)$, as a function of β, is subdominant with respect to $f_+(\xi, \beta)$ [11,34]. For this reason, the wave function in the upper half-plane of β is determined by

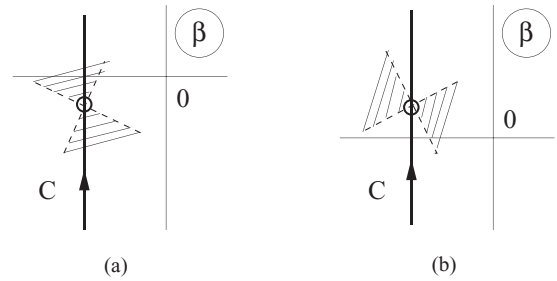

FIG. 4. The case of $1/B < r$. The saddle points are indicated by circles and the steepest descents are in the hatched parts. (a) The integration path for $f_-\varphi_-$. (b) The integration path for $f_-\varphi_+$.

$\exp(-iB\alpha\beta) f_+(\xi, \beta)\varphi(\eta, \beta)$ and the f_- part is irrelevant. The corresponding contribution is collected not from a saddle point but from a path with a strongly oscillating wave function leading to an exponentially small result.

One can note that the saddle point contribution in Fig. 4(b), which is not realized, would give a wave function which exponentially increases from the z axis that is related to the opposite sign of the second term in Eq. (50).

4. Intermediate $r \sim 1/B$

The shift of the saddle point due to finite r, as in Fig. 4, is within the semiclassical accuracy at $r \sim 1/B$. The same is valid for rotation of the steepest descent direction. This means that the both parts in Eq. (25) are of the same order with the exponential accuracy. The sum of these contributions turns to zero at some points in the $\{r, z\}$ plane. These point can be treated as vortex cores similar to vortices in superconductors when the phase is changed by 2π after circulation around the core [36]. According to the axial symmetry of the problem, vortices have the form of rings around the z axis.

The modulus of the wave function in the $\{r, z\}$ plane has a set of zeros separated by the distance of the order of $1/B$, which is the de Broglie wave length in ordinary units.

5. Summary

The true wave function has no singularity on the z axis and is not semiclassical close to it, at $r < 1/B$. At larger r it becomes semiclassical and has a tendency to form two branches, increasing and decreasing with r. It was shown that the increasing branch is irrelevant since it is dominated by the wave function strongly oscillating as a function of β. Due to the mutual interference of contributions with different β, in place of the increasing branch there is an exponentially small result. But the decreasing branch survives. As a result, the true wave function is localized near the z axis. In Appendix B a simple model is considered where vanishing, due to interference, of the increasing branch under the barrier is shown in a straightforward manner.

At the region $z < z_s$ features of the wave function can be summarized in the following way. At $r < 1/B$ it is given by Eq. (53). At $r \sim 1/B$ the wave function is characterized by the set of vortex rings around the z axis. At $1/B < r$ there

is the exponential decay from the z axis corresponding to the semiclassical approximation.

One can emphasize that these conclusions are drawn on the basis of exact analytical properties of the wave function. The semiclassical approach is used close to the saddles only.

C. Crossing the plane $\{z = 0\}$ by the flux ψ_I

Another region, where there is no flux in the classical limit, is a vicinity of the Coulomb center at $z = 0$. As follows from Eq. (29), on the plane $\{z = 0\}$, that is at $\xi = \eta = r$, the parameter β satisfies the equation

$$r[1 + 2\sqrt{\beta(1+\beta)}\sinh\alpha] = -\beta(1+\beta)\cosh^2\alpha \qquad (54)$$

and, according to Eqs. (31)–(34),

$$\begin{aligned} \frac{\partial\sigma_1}{\partial z} &= -\tanh\alpha - \frac{i}{\sqrt{r}}, \quad z = 0, \quad r \ll 1, \\ \frac{\partial\sigma_1}{\partial r} &= -\tanh\alpha + \frac{i}{\sqrt{r}}. \end{aligned} \qquad (55)$$

We see that the wave function ψ_I increases with z near the line $z = 0$. Close to the left cusp, $\{z = -z_s, r = 0\}$, the parameter $\beta = -1$ and, as follows from the relation (28) for σ_1,

$$|\psi_I(z = -z_s, r = 0)| \sim |\psi_I(z = z_s, r = 0)| \exp\left(-\frac{\pi B}{2}\right). \qquad (56)$$

The exponential comes from the η integration from 0 to 1.

The caustics D_1 and B_3 are connected by classical paths, as shown in Fig. 2. For this reason $|\psi_I|$ is the same (with the exponential accuracy) on these caustics. The analogous statement is valid for caustics D_3 and B_1, indicated in Fig. 2 by the dashed curves, where $|\psi_I|$ is exponentially small according to Eq. (56). So $|\psi_I|$ exponentially decays at negative z.

VIII. DISTRIBUTION OF THE FLUX ψ_{II}

The branch ψ_{II} is determined by Eq. (20). We do not analyze here all details of ψ_{II}, which is similar to ψ_I.

The caustics for the function ψ_{II} are shown in Fig. 5 where ones with exponentially small ψ_{II} are related to dashed curves. The caustics are of the same form as in Fig. 2. The analog of the curve R of Fig. 2 exists in Fig. 5 in a symmetric way at negative z (not shown in Fig. 5). For the branch $1b$ of ψ_I at $z_s < z$ currents j_z and j_r are negative. For the analogous branch of ψ_{II} at $z < -z_s$ the current j_z is also negative but j_r is positive. This is indicated in Figs. 2 and 5. For both cases the function $\beta(\xi, \eta)$ is the same. The relation, analogous to Eq. (56), for the branch ψ_{II} contains the opposite sign of the exponential. So the branch ψ_{II} exponentially decreases at positive z.

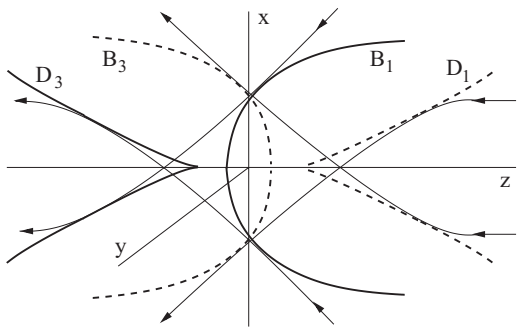

FIG. 5. Distribution of the particle flux associated with the wave function ψ_{II}. On the dashed caustics ψ_{II} is exponentially small.

The branch ψ_I is exponentially small on the dashed caustics in Fig. 2. The same is true for the branch ψ_{II} on the dashed caustics in Fig. 5. The sum of the two functions provides the same (with exponential accuracy) modulus of the total wave function on all caustics. This corresponds to experimental conditions when the far incident flux is separated due to Coulomb forces by two regions restricted by caustics D_1 and B_1. The flux is the same (with the exponential accuracy) at these regions.

IX. HOW THE PARTICLE APPROACHES THE COULOMB CENTER

The flux on the Coulomb center comes from the right (ψ_I) and goes to the left (ψ_{II}). The modulus of the total wave function (24) is a constant (with the exponential accuracy) on all caustics in Figs. 2 and 5, as stated in Sec. VIII. The curves of classical velocities in these figures are symmetric with respect to the x axis. The wave function exponentially decays inside the shadow sides of caustics. The shadow side of the caustics D_1 and B_1 is between them. The same is valid for the caustics D_3 and B_3. The branches $\sigma_{1,2,3}$ describe the whole flux distribution. The branch σ_4 does not contribute to the semiclassical wave function since a proper saddle point is absent. In other words, all classical paths, described by σ_4, interfere down to zero not very close to the z axis.

Since we are interested in the region close to the Coulomb center, details of the flux, reflected from the caustics B_1 and B_3, are not important for this purpose. Therefore we focus on σ_1 at small r.

At $r \sim z \ll 1$ Eq. (29) can be easily solved since in this case the parameter $1 + \beta$ is small. The result is

$$\begin{aligned} \frac{\partial\sigma_1}{\partial z} &= -\frac{2\xi}{\xi+\eta}\tanh\alpha - \frac{2i\sqrt{\eta}}{\xi+\eta}, \quad r \sim z \ll 1, \\ \frac{\partial\sigma_1}{\partial r} &= -\frac{2\sqrt{\xi\eta}}{\xi+\eta}\tanh\alpha + \frac{2i\sqrt{\xi}}{\xi+\eta}, \end{aligned} \qquad (57)$$

which also corresponds to decrease of the wave function inside the shadow region. The continuity equation $\operatorname{div}\vec{j} = 0$ in the semiclassical approximation is equivalent to Ref. [11]

$$(\nabla \operatorname{Im}\sigma)(\nabla \operatorname{Re}\sigma) = 0, \qquad (58)$$

that is, the momentum $\nabla \operatorname{Re}\sigma$ is directed along a curve of constant $|\psi|$ as in Fig. 6. One can check that expressions (49) and (57) satisfy the condition (58).

In Fig. 6 the local angle χ between the tangent direction of the curves $c_{1,2}$ (see Fig. 6) and the z axis is given by the

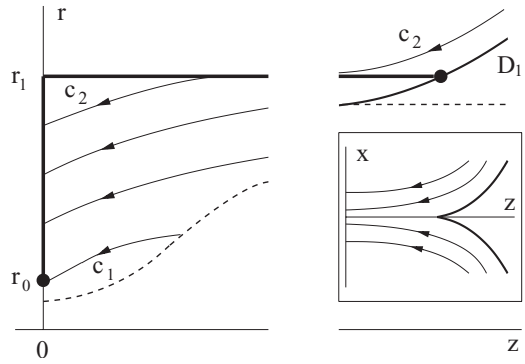

FIG. 6. Curves c_1, c_2, and others of constant $|\psi|$ are also directions of momenta. The semiclassical approximation is not valid below the dashed curve described in the text. The left part of the interrupted plot is related to small z. The inset shows in the $\{x, z\}$ plane how the flux gets away from the cusp and moves to the Coulomb center (cusp driven tunneling).

relation

$$\frac{\partial \operatorname{Im}\sigma}{\partial r}\tan\chi = -\frac{\partial \operatorname{Im}\sigma}{\partial z}. \tag{59}$$

As follows from Eqs. (49) and (57), at $r \ll 1$

$$\begin{aligned} \tan\chi &= \frac{r z_s}{2z(z_s - z)}, \quad r \ll z < z_s, \\ \tan\chi &= \left(\frac{\sqrt{r^2+z^2}-z}{\sqrt{r^2+z^2}+z}\right)^{1/2}, \quad r \sim z \ll 1. \end{aligned} \tag{60}$$

According to these equations, the curves c_1, c_2, and others in Fig. 6 are directed by 45° with respect to the r axis at $z = 0$. At $z \sim 1$ these curves are almost parallel to the z axis.

Another important aspect is a border of applicability of the semiclassical approximation used. This approximation holds when the terms with quantum corrections [ones with second derivatives in Eq. (13)] to the Hamilton-Jacobi equation are small. Substituting expressions (49) and (57) into Eq. (13), one can approximately conclude that the semiclassical approximation is violated below the dashed curve in Fig. 6, which is $r \sim 1/B^2$ at $z < 1/B$, $r \sim \sqrt{z}/B$ at $1/B^2 < z < 1/2$, and $r \sim 1/B$ at larger z. In physical units the scale $1/B$ corresponds to the de Broglie wavelength defined in Sec. II. The scale $1/B^2$ is the Bohr radius (Sec. II) which is the shortest spatial scale of the Coulomb problem. As it should be, the semiclassical approximation is not valid too close to the z axis [11].

We make a remark on validity of the semiclassical approximation. Strictly speaking, this approach is valid at $1/B < z$ and $1/B < r$ where β fluctuations around the saddles are Gaussian and small. When $z < 1/B$, fluctuations of β become large, of the order of $1 + \beta$; that is, non-Gaussian. According to this, at $z = 0$ the first two terms (classical and quantum) in Eq. (13) become of the same order $\sim 1/B^2 r$. The third term (classical) is of the order of unity and the forth one (quantum) is proportional to $1/B\sqrt{r}$.

One can say that the total energy is redistributed in such a way as to be mainly defined by the momentum in the η direction. For this reason, at $1/B < r$ one can apply the semiclassical approach in the η subsystem which determines the wave function with exponential accuracy. Non-Gaussian fluctuations in the ξ subsystem influence a preexponential factor only. Details of these calculations will be published elsewhere.

The inset in Fig. 6 shows the flux flow in the shadow region of the caustic D_1. According to general properties of caustics, $|\psi_1|$ decays on the shadow side away from D_1. Arrowed curves close to the caustic D_1 in the inset in Fig. 6 relate to constant $|\psi_1|$. The closer the curve is to D_1 the larger $|\psi_1|$ is. The same is valid approaching the z axis in the region left from the cusp, where the modulus of the wave function reaches its maximal value close to the z axis. That value is kept along the whole segment of the z axis, from the cusp to the center.

The caustic D_1 in Fig. 6 is associated with branch 1 of ψ_I. The analogous branch (related to ψ_{II}) is connected with the caustic D_3 in Fig. 5 and supplements Fig. 2 by the mirror reflection. In this way, the flux is continued from positive to negative z. So the particle flux in Fig. 2, from the caustic D_1 to D_3, is localized at the narrow channel around the z axis. This can be called cusp driven tunneling.

The same type of channel, analogous to the wave ψ_1 to the left from the cusp, is associated with a cusp caustic in optics and acoustics. It coexists with the wave, analogous to ψ_2, which escapes from the cusp caustic piercing it. In Appendix A both types of rays in optics are demonstrated. This correlates with numerical studies done in Ref. [37] where interference oscillations in the total amplitude of $\psi_1 + \psi_2$ are extended far to the left from the cusp. These oscillations are unavoidable since they result from topological properties; namely, dislocations in the spatial distribution of the total light amplitude [37]. Without the channel it would be solely the wave, analogous to ψ_2, which does not lead to the interference oscillations. At large distances from the cusp, the channel is smeared out in space due to non-semiclassical effects. In our case such distances are not involved since the center is close to the cusp.

The tunneling probability can be defined with exponential accuracy as the ratio of densities at the center and at large distances,

$$w \sim \left|\frac{\psi(r_0, 0)}{\psi(r_1, \infty)}\right|^2. \tag{61}$$

The parameters r_0 and r_1 are indicated in Fig. 6. The point $\{r_0, 0\}$ is not exactly at the center but when $r_0 \sim 1/B^2$ the expression (61) does not differ from the exact probability in the exponential approximation. The tunneling probability has the form

$$w \sim \exp\left\{-2B \operatorname{Im}\left[\sigma_1(r_0, 0) - \sigma_1(r_1, \infty)\right]\right\}. \tag{62}$$

The infinity point can be substituted by one on the caustic D_1 as shown in Fig. 6 since σ is real to the right from the caustic.

If in the expression (62) $1/B^2 < r_0 < r_1$ and $1/B < r_1$ then one can use the semiclassical approximation along the path (two thick lines) between the two dots in Fig. 6. For convenience, we take in addition $r_1 \ll 1$. Then the first equation (57) simply gives

$$\operatorname{Im}\left[\sigma_1(r_1, \infty) - \sigma_1(r_1, 0)\right] = -2\sqrt{r_1}. \tag{63}$$

The second equation (57) produces

$$\mathrm{Im}\,[\sigma_1(r_1,0)-\sigma_1(r_0,0)]=2\sqrt{r_1}-2\sqrt{r_0}. \qquad (64)$$

By means of Eqs. (62)–(64) the ratio of densities at points $\{r_0,0\}$ and $\{r_1,\infty\}$ in Eq. (61) can be written in the form

$$w\sim\exp\left(-4B\sqrt{r_0}\right). \qquad (65)$$

Equation (65) holds when $1/B^2<r_0$, and formally that expression is exponentially small. It is clear that one can continue r_0 down to the border of applicability of the result (65), namely to put $r_0\sim 1/B^2$. One can conclude from here that tunneling probability is not exponentially small.

It is shown in this section that the semiclassical solution may be tracked along some paths in Fig. 6 from the classically allowed region to one close to the Coulomb center. Formally, the semiclassical wave function remains exponentially small on those paths. It corresponds to the true wave function outside the nuclear Bohr radius. Below the Bohr radius the semiclassical approach is not valid and the wave function is not exponentially small. But the Bohr radius is only a few times larger than the region of nuclear forces 4.256×10^{-13} cm [38], and therefore the wave function does not substantially differ between these distances.

According to Sec. IV, the wave function in the classically allowed region is inversely proportional to the radius, providing conservation of the total incident flux. Since close to the cusp the channel radius is $\sim 1/B$, the fraction $1/B^2$ of the total incident flux gets away from the cusp and moves along the channel. This fraction reaches the vicinity of the Coulomb center where the channel radius becomes of the Bohr radius. So the probability $w\sim 1/B^2$ substitutes the WKB one, $\exp(-\pi B)$, related to the case of a plane incident wave.

X. INCIDENT FLUX FAR FROM THE COULOMB CENTER

In the absence of the Coulomb potential the flux from the left to the right relates to $\sigma=-2z$ and consequently to the plane wave $\psi=\exp(-2iBz)$ in the whole space. If we add the Coulomb potential that plane wave is hardly influenced far to the right but becomes strongly violated at finite distances. In particular, the caustic is formed as shown in Fig. 1. This situation corresponds to $\beta=-i/B$ as mentioned in Sec. III.

Suppose again that the Coulomb potential is absent but the incident flux from the right is not a plane wave but one related to $\sigma=-z\tanh\alpha\pm r/\cosh\alpha$. The corresponding exact wave function is expressed through the Bessel function

$$\psi=\exp(-2iBz\tanh\alpha)J_0\left(\frac{2Br}{\cosh\alpha}\right). \qquad (66)$$

In this case the velocity distribution is shown in Fig. 7(a).

If we add the Coulomb potential the velocity field becomes strongly deformed. The new velocity distribution is illustrated in Fig. 7(b) where

$$\cot\theta_0=\sinh\alpha. \qquad (67)$$

It is easy to qualitatively understand the features of that distribution. The flux, locally parallel as in Fig. 7(a), is reflected by the Coulomb force upward when the polar angle

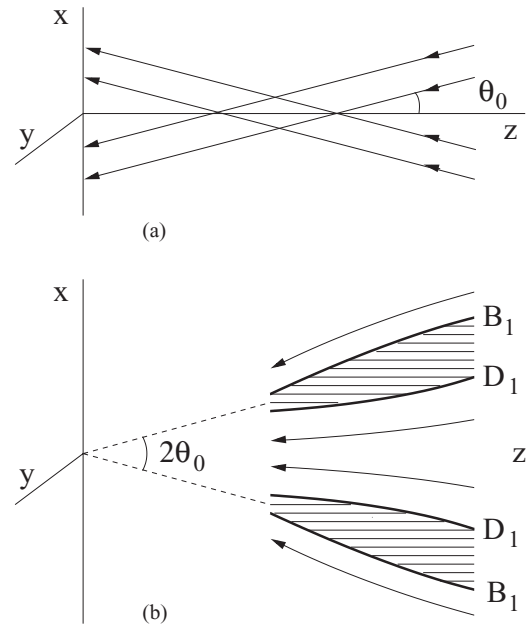

FIG. 7. (a) Conical particle flux from the right in the absence of the Coulomb potential. (b) Split of the conical flux by the Coulomb field at large z. Trajectories are reflected from caustics which are continuations of ones in Fig. 2. The dashed parts are caustic shadows.

θ ($\tan\theta=r/z$) exceeds θ_0. This flux is reflected downward when θ is less than θ_0. The shadow region is between these limits as in Fig. 7(b).

If n is a direction normal to a caustic surface then the wave function decays inside the shadow region as

$$\psi\sim\exp[-(n/l)^{3/2}], \qquad (68)$$

where $l\sim(\lambda^2 z)^{1/3}$ in physical units. Here λ is the wavelength defined in Sec. II. Equation (68) is a usual form for caustics [12]. As follows from Eqs. (37) and (39), the distance between caustics D_1 and B_1 at large z is proportional, in physical units, to $\sqrt{ze^2/E}$ which is larger than l. So there is a real shadow between the caustics.

We see that properties of the incident flux at large distances strongly determine the wave function at the Coulomb center.

XI. DISCUSSIONS

Probability of tunneling across a one-dimensional static potential barrier is exponentially small when the barrier is almost classic. The wave function decays inside the barrier since in the classically forbidden region the wave vector is imaginary.

Below some nonrigorous arguments are given. When dimensionality of a problem is higher than 1 the situation can be more complicated since the wave vector has more than one components in space. The sum of squared components, which is a kinetic energy, is negative under the barrier. In the classical manner this can be written in the form [compare with

Eq. (11)]

$$k_r^2 + k_z^2 + \frac{1}{2\sqrt{r^2+z^2}} = 1. \tag{69}$$

In our case the z axis is the tunneling direction and tunneling probability is determined by $\mathrm{Im}\, k_z$. The smaller is this value the larger is the probability. Equation (69) formally says that a reduction of $\mathrm{Im}\, k_z$ is connected with increasing of $\mathrm{Im}\, k_r$.

A localization near the z axis is equivalent to a large $\mathrm{Im}\, k_r$ at that region and therefore leads to increase of tunneling rate along the z direction. A localization of the density around the z axis is possible but, as a "payment" for this, the wave function has a nonphysical singularity on that line. Therefore one has to add the second branch to compensate the singularity. But the second branch exponentially increases away from the z axis, which violates, at the first sight, the construction.

The above statement holds when some particular value of k_r is chosen. If we consider a continuous set of waves with various k_r, properties of the resulting wave function can be completely different. This is exactly our case. Due to an interference in the set of second branches, they compensate each other at finite r, except in a narrow (non-semiclassical) region in the vicinity of the z axis. As a result, only the state decaying from the z axis (channel) survives. A simple example of this phenomenon is considered in Appendix B. An analogous channel is associated with a cusp caustic in optics and acoustics due to the similar phenomenon of getting away from a caustic cusp. Some details are in Appendix A.

The method used in this paper is based on analytical properties of the wave function in the β complex plane. The semiclassical approximation for the wave function is applied in vicinities of the saddle points only. Exact analytical properties allow us to select solely the saddles contributing to the integration.

To get a cusp caustic one should have a convergent incident wave at large distances. In our case the cusp position on the z axis, $e^2/(E\sin^2\theta_0)$, is determined by the characteristic angle θ_0 of the incident conical flux. When the incident flux is just a plane wave, as in the conventional scattering problem, there is no cusp caustic. In this case only the usual one exists, as in Fig. 1.

An origin of the cusp is based on global properties of the flux. The Coulomb field separates the incident conical flux, with the characteristic angle θ_0 in Fig. 7(a), according to geometrical rules. Namely, all rays with larger angles are turned upward and ones with smaller angles are turned downward. This is equivalent to a separation of the two streams by caustics. In continuation toward the Coulomb center, the internal caustic shrinks to a cusp point on the z axis before the center. Otherwise the flux classically reaches the Coulomb center. The flux gets away from the cusp and moves to the center along the above channel containing the z axis. Not too close to the center the radius of the channel is proportional to de Broglie wavelength.

This is cusp driven tunneling when the cusp forms the flux on the Coulomb center. In the vicinity of the center the flux passes the bottleneck of the size of the nuclear Bohr radius. This happens since close to the center the de Broglie wavelength is no longer a relevant spatial scale which becomes the Bohr radius. Then at negative z the flux moves to the left. Since interference effects are essential the proper nuclear reaction can be called coherent fusion.

The fusion probability is proportional to a neutron yield. The neutron yield of the process depends on the weight function $c_I(\beta)$ (19) and, therefore, on details of the incident flux. With the choice (20) the yield is not exponentially small as $\exp(-6174.9)$ (Sec. II) but it can be "normally" small due to a preexponential factor in the tunneling probability. One can increase this factor by variation of a prefactor in the weight function (20).

We consider in the text the axially symmetric wave function of two deuterons related to the magnetic quantum number $m = 0$. A finite m reduces the effect due to formation of a centrifugal repulsive barrier.

In this paper we briefly mention experimental schemes for formation of a particle flux resulting in the cusp phenomenon.

One of experimental ways to produce the conical flux of deuterons (66), shown in Fig. 4(a), is to confine them in a long tube with rigid walls; for example, in a nanotube. Another way is to push deuterons (atoms) to pass through a diffraction grid of a conical shape. Since the de Broglie wavelength is of the order of 1 Å, one can use a natural crystal lattice. A setup with slits also can be used. This is a case of a quantum lens. We will discuss the details elsewhere.

Above, two bare deuterons are considered. From a practical standpoint it can be more convenient to deal with a substance (heavy water, for example) consisting of molecules with deuterium. Inside a single molecule of heavy water the deuterons are in the well with vibration energy levels. An external laser radiation can influence a quantum state of deuterons in the well. One can pose the question whether the radiation is able to create something like a cusp state in the well and which pulse shape should be used for this purpose.

Formation of a required particle flux in experiments requires a detailed study, which is outside the scope this paper.

XII. CONCLUSIONS

Fusion of two bare (supposedly isolated from everything) deuterons of room-temperature energy is possible. The penetration across the Coulomb barrier, which is the main obstacle for low-energy fusion, strongly depends on a form of the incident flux on the center at large distances from it. In contrast to the usual scattering, the incident wave is not a single plane wave but a superposition of plane waves of the same energy and various directions; for example, a convergent conical flux. As a result of interference, the wave function close to the Coulomb center is determined by the cusp caustic which is probed by de Broglie waves. The particle flux gets away from the caustic cusp and moves to the Coulomb center providing a not small probability of fusion (cusp driven tunneling).

ACKNOWLEDGMENTS

The author is grateful to P. Cooper, J. Engelfried, and M. Kirchbach for discussions of related topics.

APPENDIX A: CHANNEL FORMATION IN OPTICS

A cusp caustic is possible also in optics. See, for example, Ref [37]. Rays get away from the cusp as in Fig. 6 and propagate to the left within a narrow channel. Below, this phenomenon is studied. We consider for simplicity a two-dimensional problem described by the dimensionless equation

$$\frac{1}{B^2}\left(\frac{\partial^2\psi}{\partial z^2}+\frac{\partial^2\psi}{\partial x^2}\right)+\psi=0, \tag{A1}$$

where ψ denotes a component of an electromagnetic field and the scale $1/B$ corresponds to the de Broglie wavelength.

A solution at positive x can be written in the form

$$\psi(z,x)=\int_C dk\exp\left(-iBz\sqrt{1-k^2}-\frac{iB}{4}k^4\right)\times[\exp(iBkx)+\exp(-iBkx)], \tag{A2}$$

where C is the contour in the complex plane of k shown in Fig. 8. Equation (A2) is an exact solution of Eq. (A1). It was numerically analyzed in Ref. [37]. Here we emphasize important features of the solution.

Small z and x are considered below. Accordingly, the saddle point in Eq. (A2) relates to small k. The saddle point, corresponding to $\exp(-iBkx)$ in Eq. (A2), is determined by the equation

$$k^3-zk+x=0. \tag{A3}$$

A branch point of the solution defines the caustic

$$x=\frac{2}{3}\left(\frac{z}{3}\right)^{3/2}, \tag{A4}$$

which is analogous to Eq. (36). See also Fig. 6. At negative z and small x the saddle points are (see Fig. 8)

$$k_{s1}=-i\sqrt{-z}-\frac{x}{2z},\quad k_{s2}=\frac{x}{z}. \tag{A5}$$

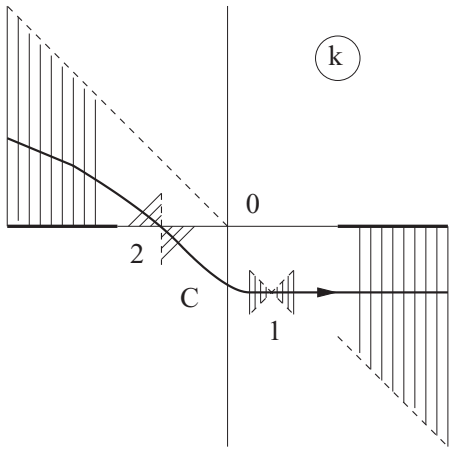

FIG. 8. Far ends of the integration contour C in Eq. (A2) are in the dashed regions where the wave function exponentially decreases. The dashed line is tilted by an angle of 45°. The contour passes along steepest descents of the saddles which are at the dashed regions close to the saddle points 1 and 2. The thick lines are cuts connected to the function $\sqrt{1-k^2}$.

There is also the saddle point which is the complex conjugation of k_{s1} but it does not contribute to the integration along C.

If to take $\exp(-iBkx)$ in Eq. (A2) there are also two saddles contributing to the integration along C. The saddle points are $-k_{s1}$ and $-k_{s2}$. The total result is a sum of two branches $\psi_1+\psi_2$ where, at negative z and small α,

$$\psi_1(z,x)\sim\exp(-iBz-B|x|\sqrt{-z}) \tag{A6}$$

and

$$\psi_2(z,x)\sim\exp\left(-iBz-\frac{iBx^2}{z}\right). \tag{A7}$$

Eq. (A6) is valid at $1/B<|x|$. The exact solution does not have the singularity at $x=0$. The branch (A6) is analogous to Eq. (50) and corresponds to rays which get away from the cusp as in Fig. 6. The branch (A7) is analogous to the branch 2 at $1/2<z<z_s$ in Sec. VI.

APPENDIX B: CHANNEL UNDER THE BARRIER

In Sec. VII B the channel under the Coulomb barrier is investigated. It is described by the wave function weakly decaying along the z axis and localized close to it. This type of solution can be simply constructed using arguments given by Eq. (69). One can take a function, weakly decaying along the z axis (small k_z), which permanently decreases in the perpendicular direction r (a finite imaginary k_r). This function, exponentially decaying in the r direction at large r, should have the unphysical singularity $\ln r$ at small r, reminding us of the Bessel function $K_0(Br)$ [39] with the same properties. This type of unphysical wave function is clear despite the underbarrier region being involved.

The problem is to eliminate the singularity at small r. For this purpose another branch has to enter the game to compensate the singularity. So the total solution becomes smooth at small r but is expected to exponentially increase at large r analogous to the Bessel function $I_0(Br)$ [39]. The statement of Sec. VII B is that if we take the infinite set of functions, the exponentially increasing branch disappears due to mutual interference.

In the Coulomb problem, vanishing of the increasing branch is accompanied by specific details. Below we propose a simple model where details do not mask how the interference kills the increasing branch. We use the two-dimensional Schrödinger equation

$$-\frac{1}{B^2}\left(\frac{\partial^2\psi}{\partial z^2}+\frac{\partial^2\psi}{\partial x^2}\right)=-\psi, \tag{B1}$$

which describes an underbarrier motion in dimensionless units. The scale $1/B$ relates to the de Broglie wavelength. The exact solution of Eq. (B1) has the form

$$\psi(z,x)=\int_{-\infty}^{\infty}dk\exp\left(Bz\sqrt{1+k^2}+iBkx-\frac{B\alpha}{2}k^2\right), \tag{B2}$$

which is smooth at $x=0$. The parameter B is large and α is, generally, of the order of unity.

Even without calculations one can draw a conclusion that the function (B2) is localized close to the z axis at all z (the channel). Indeed, at $x = 0$ the function (B2) is determined by the saddle method. For example, at negative z the saddle point is $k_s = 0$. At a finite $x > 1/B$ the additional rapidly oscillating exponent can only reduce the result of integration of the Gaussian function.

Since B is large one can apply a saddle method to evaluate the integral. The saddle point in Eq. (B2) is given by the expression

$$\alpha k - \frac{zk}{\sqrt{1+k^2}} = ix. \tag{B3}$$

To be specific we consider negative z and small α. Then the saddle position is $k_s = ix/\sqrt{z^2+x^2}$ which results in the wave function

$$\psi(z,x) \sim \exp(-B\sqrt{z^2+x^2}), \quad z < 0. \tag{B4}$$

The formula (B4) is valid when ψ is exponentially small.

The solution (B2) is not singular and it exponentially decreases at large $|x|$. At positive z the solution is different but also corresponds to a channel localized near the z axis. This means that at a fixed z (negative or positive) the wave function exponentially decreases with increase of $|x|$.

In the considered limit $\alpha \ll 1$, Eq. (B4) looks similar to the exact solution of Eq. (B1), $I_0(B\sqrt{z^2+x^2})$, if we artificially "cut off" its exponentially increasing part $\exp(B\sqrt{z^2+x^2})$ at large distances. That Bessel function follows from Eq. (B2) if we change the weight function $\exp(-iB\alpha k^2/2) \to 1/\sqrt{1+k^2}$ and integrate around the cut $\{-i, i\}$ in the complex plane of k [39].

One can see that the asymptote far from the z axis crucially depends on the choice of the integration contour in Eq. (B2); in other words, on the way of adding partial waves with different k. The formula (B2) is constructed in a manner to naturally remove the increasing exponent due to interference of partial waves. The same can be said about the choice of the integration contour in Fig. 4.

The exact solution (B2) is analogous to the exact solution (51) for the Coulomb field. Both describe channels in classically forbidden regions. Due to distinctions in physical systems (for example, in the presented model the underbarrier region is infinitely long) the wave function decays more weakly under the Coulomb barrier. This difference has a secondary meaning compared to the main common feature: vanishing of the increasing branch, from the z axis, due to interference.

[1] R. Herman, *Fusion: The Search for Endless Energy* (Cambridge University Press, Cambridge, 1990).
[2] G. Taubes, *Bad Science: The Short Life and Weird Times of Cold Fusion* (Random House, New York, 1993).
[3] E. Storms, *The Science of Low Energy Nuclear Reactions* (World Scientific, Singapore, 1993).
[4] K. Czerski, A. Huke, A. Biller, P. Heide, and G. Ruprecht, Europhys. Lett. **54**, 449 (2001).
[5] B. Naranjo, J. K. Gimzewski, and S. Putterman, Nature (London) **434**, 1115 (2005).
[6] A. Widom and L. Larsen, Eur. Phys. J. C **46**, 107 (2006).
[7] A. Huke, K. Czerski, P. Heide, G. Ruprecht, N. Targosz, and W. Zebrowski, Phys. Rev. C **78**, 015803 (2008).
[8] E. Sheldon, Contemp. Phys. **49**, 375 (2009).
[9] Y. E. Kim, J. Cond. Matter Nucl. Sci. **4**, 188 (2011).
[10] E. Storms, J. Cond. Matter Nucl. Sci. **9**, 1 (2012).
[11] L. D. Landau and E. M. Lifshitz, *Quantum Mechanics* (Pergamon, New York, 1977).
[12] L. D. Landau and E. M. Lifshitz, *The Classical Theory of Fields* (Butterworth-Heinemann, Oxford, 1998).
[13] B. Ivlev, arXiv:1207.2357.
[14] B. Ivlev, arXiv:1211.1243.
[15] L. D. Landau and E. M. Lifshitz, *Mechanics* (Pergamon, New York, 1977).
[16] B. Ivlev, Ann. Phys. **326**, 979 (2011).
[17] B. Ivlev, arXiv:1108.5146.
[18] B. Ivlev and J. P. Palomares-Báez, Phys. Rev. B **82**, 184513 (2010).
[19] J.-L. Gervais and B. Sakita, Phys. Rev. D **16**, 3507 (1977).
[20] A. J. Leggett, *Tunneling in Complex Systems* (World Scientific, Singapore, 1998).
[21] E. J. Heller, J. Phys. Chem. A **102**, 10433 (1999).
[22] T. Sharpee, M. I. Dykman, and P. M. Platzman, Phys. Rev. A **65**, 032122 (2002).
[23] J. Ankerhold, *Quantum Tunneling in Complex Systems* (Springer-Verlag, Berlin, 2007).
[24] C. G. Callan and S. Coleman, Phys. Rev. D **16**, 1762 (1977).
[25] S. Coleman, *Aspects of Symmetry* (Cambridge University Press, Cambridge, 1985).
[26] A. Schmid, Ann. Phys. **170**, 333 (1986).
[27] U. Eckern and A. Schmid, in *Quantum Tunneling in Condensed Media*, edited by A. Leggett and Yu. Kagan (North-Holland, Amsterdam, 1992).
[28] B. Ivlev, Phys. Rev. A **70**, 032110 (2004).
[29] J. P. Palomares-Baez, B. Ivlev, and J. L. Rodriguez-Lopez, Phys. Rev. A **76**, 052103 (2007).
[30] B. Ivlev and V. Gudkov, Phys. Rev. C **69**, 037602 (2004).
[31] V. De Alfaro and T. Regge, *Potential Scattering* (North Holland, Amsterdam, 1965).
[32] C. DeWitt-Morette, B. Nelson, and T.-R. Zhang, Phys. Rev. D **28**, 2526 (1983).
[33] N. Grama, C. Grama, and I. Zamfirescu, J. Phys. A **42**, 465306 (2009).
[34] J. Heading, *An Introduction to Phase-Integral Methods* (John Wiley, London, 1962).
[35] V. I. Arnold, *Singularities of Caustics and Wave Fronts* (Kluwer Academic, Dordrecht, 1990).
[36] P. G. de Gennes, *Superconductivity of Metals and Alloys*, (Addison-Wesley, Reading, MA, 1966).
[37] M. Berry, in *Huygens' Principle 1690–1990: Theory and Applications*, edited by H. Blok, H. A. Ferwerda, and H. K. Kuiken (Elsevier Science, Amsterdam, 1992).
[38] R. Pohl *et al.*, J. Phys.: Conf. Ser. **264**, 012008 (2011).
[39] I. S. Gradshteyn and I. M. Ryzhik, *Table of Integrals, Series, and Products* (Academic, New York, 1980).